

Low-Temperature Ammonia Synthesis on Iron Catalyst with an Electron Donor

Masashi Hattori, Natsuo Okuyama, Hiyori Kurosawa, and Michikazu Hara*



Cite This: *J. Am. Chem. Soc.* 2023, 145, 7888–7897



Read Online

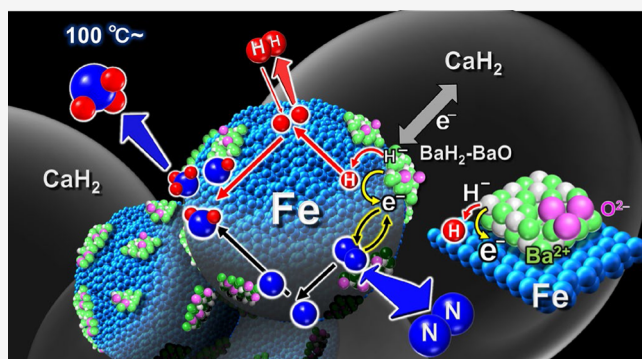
ACCESS |

Metrics & More

Article Recommendations

Supporting Information

ABSTRACT: Haber–Bosch process produces ammonia to provide food for over 5 billion people; however, it is currently required to be produced without the use of fossil fuels to reduce global CO₂ emissions by 3% or more. It is indispensable to devise heterogeneous catalysts for the synthesis of ammonia below 100–150 °C to minimize the energy consumption of the process. In this paper, we report metallic iron particles with an electron-donating material as a catalyst for ammonia synthesis. Metallic iron particles combined with a mixture of BaO and BaH₂ species in an appropriate manner could catalyze ammonia synthesis even at 100 °C. The iron catalyst revealed that iron can exhibit a high turnover frequency ($\sim 12 \text{ s}^{-1}$), which is over an order of magnitude higher than those of other transition metals used in highly active catalysts for ammonia synthesis. This can be attributed to the intrinsic nature of iron to desorb adsorbed hydrogen atoms as hydrogen molecules at low temperatures.



1. INTRODUCTION

The low ammonia yield has been a significant issue in the Haber–Bosch (HB) process for over 100 years. The maximum ammonia yield at equilibrium decreases with increasing reaction temperature in the HB process (Figure 1). The

has pushed recent research toward low-temperature ammonia synthesis.

Most of the recently reported highly active catalysts use Ru, Co, and Ni as reaction sites because these can be easily deposited on supports as highly dispersed metal nanoparticles that exhibit high catalytic performance.^{7–11} While we have also discovered a unique Ru-based heterogeneous catalyst to synthesize ammonia from H₂ and N₂, even below 100 °C,¹² we have questioned whether catalysts that use these transition metals have significant potential to increase the catalytic activity at the desired reaction temperature of $\leq 100\text{--}150$ °C from the perspective of the H₂ adsorption/desorption equilibrium. The dissociative adsorption of H₂ and H₂ desorption from the resulting adsorbed H atoms (H adatoms) are in equilibrium on all transition metal surfaces in the synthesis of ammonia as well as N₂ adsorption/desorption. It is well known for Ru catalysts that adsorption of H adatoms onto the transition metal surfaces is preferential so that the H₂ adsorption/desorption equilibrium shifts toward H₂ adsorption, which decreases ammonia formation by the decrease in adsorption sites for N adatoms.^{13,14} Such hydrogen-poisoning

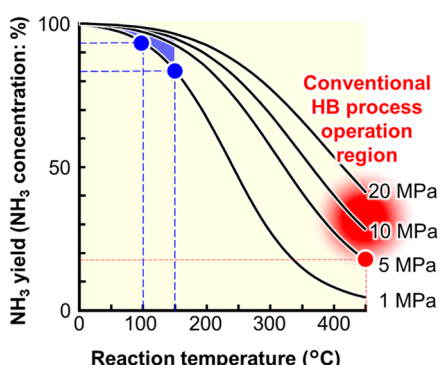


Figure 1. Correlation of ammonia yield with temperature and pressure.

operating temperature for the iron-based catalyst used in the present process exceeds 400 °C, which requires pressurization of the process to ~ 20 MPa to obtain a yield of 30–40% at most.^{1–6} However, any catalyst that could allow the operating temperature to be decreased below 100–150 °C would significantly increase the ammonia yield. Therefore, this issue

Received: December 7, 2022

Published: March 30, 2023



can affect all transition metals used in the synthesis of ammonia. Attributing hydrogen-poisoning to the bond strength between H adatoms and the surface transition metal atoms, it is anticipated that this effect is enhanced with a decrease in ammonia synthesis temperature because a larger amount of H adatoms would be more tightly adsorbed on the transition metal surfaces with a decrease in temperature. As a result, hydrogen-poisoning would be a major obstacle to the desirable low-temperature ammonia synthesis over catalysts that employ transition metals as the active sites.

In the present study, we have again focused on iron used as the reaction site since the beginning of the HB process. Iron has been regarded as a classical transition metal that is inferior to other transition metals for ammonia synthesis. Several catalysts that use other transition metals exhibit much higher catalytic performance for ammonia synthesis than iron-based catalysts used in the present HB process.^{8,12} In addition, no effective ways to use iron for ammonia synthesis at low temperatures as low as 100 °C have been found to date. On the other hand, ammonia synthesis over iron-based catalysts has not been reported to be strongly influenced by hydrogen-poisoning. This suggests that the H₂ adsorption/desorption equilibrium on iron surfaces is shifted more toward H₂ desorption, and thus a decrease in the H adatom concentration than with other transition metals. Therefore, iron may be used for ammonia synthesis while preventing hydrogen-poisoning, even at low temperatures, if iron can be combined with an appropriate promoter in an appropriate manner. The use of ubiquitous, abundant, and inexpensive iron is also a significant advantage with respect to the environment and economy.

2. METHODS

2.1. Preparation of Iron Particles Loaded with and without BaH₂-BaO (BaH₂-BaO/Fe/CaH₂, Fe/CaH₂). BaH₂-BaO/Fe/CaH₂ and Fe/CaH₂ were typically prepared by heating a mixture of Ba(NO₃)₂-impregnated α-Fe₂O₃ and CaH₂ particles and a mixture of Fe₂O₃ and CaH₂ particles, respectively, in a flow of H₂. 7.0 g of Fe(NO₃)₃·9H₂O (Kanto Chemical) was dissolved in 30 mL of distilled water, which was then removed from the solution by rotary evaporation at 70 °C. The remaining red solid was heated at 300 °C for 10 h in air to yield α-Fe₂O₃ powder. For the preparation of BaH₂-BaO/Fe/CaH₂, 0.20 g of α-Fe₂O₃ and 0.052 g of Ba(NO₃)₂ (High Purity Chemicals) were stirred in 10 mL of distilled water for 30 min, and the water was then evaporated at 70 °C. The resultant Ba(NO₃)₂-impregnated α-Fe₂O₃ was heated at 300 °C for 10 h in air. In an Ar-filled glovebox, 0.023 g of Ba(NO₃)₂-impregnated α-Fe₂O₃ and 0.077 g of CaH₂ were mixed in an alumina mortar and transferred into a stainless steel fixed-bed reactor for ammonia synthesis (see Supporting Information 1.1 and Figure S1). The reactor was removed from the Ar-filled glovebox to the atmosphere and connected to a flow reaction system without exposure of the mixture in the reactor to the atmosphere. The mixture was heated in a flow of H₂ (45 mL min⁻¹) at 300 °C for 2 h, which resulted in BaH₂-BaO/Fe/CaH₂. Inductively coupled plasma (ICP) spectroscopy analysis indicated that the atomic ratio of Fe/Ba/Ca in the catalyst was 12.5:1.0:100.0. Fe/CaH₂, i.e., metallic iron particles without BaH₂-BaO were obtained from a mixture of 0.019 g of α-Fe₂O₃ and 0.081 g of CaH₂ by the same preparation procedure as that for BaH₂-BaO/Fe/CaH₂. The Fe/Ca atomic ratio in the resultant catalyst was 12.1:100.0. The size of the metallic iron particles in the catalysts was 20–40 nm (mean particle size: 26 nm).

2.2. Preparation of Ru or Iron Nanoparticles Deposited on BaH₂-BaO (Ru/BaH₂-BaO, Fe/BaH₂-BaO). According to a previous report,¹⁵ Ru/BaH₂-BaO and Fe/BaH₂-BaO were prepared from a mixture of 3 mol% BaO (Kojundo Chemical) and 97 mol% CaH₂ with Ru(acac)₃ or Fe(acac)₂ corresponding to 10 wt % Ru or Fe. The

mixture was prepared and transferred into the stainless steel fixed-bed reactor in an Ar-filled glovebox. The reactor was connected to the flow reaction system, as described in Section 2.1, and the mixture was heated at 260 °C in a flow of H₂ (2.5 mL min⁻¹). After 2 h, the samples were heated at 340 °C for 10 h in a flow of H₂ (2.5 mL min⁻¹). In the resultant materials, transition metal nanoparticles were deposited on the BaH₂-BaO phase formed on large CaH₂ particles (several micrometers).¹⁵ The transition metal particle sizes (Ru: 2–7 nm (mean particle size: 4 nm), Fe: 2–8 nm (mean particle size: 4 nm)) in the catalysts (Ru/BaH₂-BaO, Fe/BaH₂-BaO) were smaller than those (Fe: 20–40 nm (mean particle size: 26 nm)) of the catalysts (BaH₂-BaO/Fe/CaH₂, Fe particles) prepared by the method described in Section 2.1. ICP analysis indicated that the Ru/Ba/Ca and Fe/Ba/Ca atomic ratios for the Ru/BaH₂-BaO and Fe/BaH₂-BaO catalysts were 4.9:3.2:100.0 and 8.9:3.1:100.0, respectively.

2.3. Evaluation of Catalytic Performance (See Supporting Information 1.1 and Figure S1). Ammonia synthesis over each catalyst was examined in a stainless steel fixed-bed reactor (catalyst; 0.1 g) at 300 °C under a flow of N₂-H₂ (N₂ and H₂ >99.999%, N₂/H₂ = 1:3, 60 mL min⁻¹, weight hourly space velocity (WHSV): 36 000 mL g cat⁻¹ h⁻¹) at 0.9 MPa. After no increase or decrease in activity was observed for over 20 h, the catalyst was cooled down to below 20 °C in a flow of N₂ at a flow rate of 60 mL min⁻¹ and then held under this flow for 5 h. After no ammonia formation was confirmed, the catalyst was heated at specific temperatures in a flow of N₂-H₂. The ammonia produced was trapped in 5 mM H₂SO₄ aqueous solution, and the amount of NH₄⁺ generated in the solution was estimated using an ion chromatograph (LC-2000 plus, Jasco) equipped with a thermal conductivity detector. The rate of ammonia formation was repeatedly measured more than three times after the ammonia formation rate remained constant for over 1 h. It was verified that the measured rate of ammonia formation had an error of less than 5%.

Time of flight (TOF) was calculated from the ammonia formation rate, and the number of surface zero-valent transition metal atoms (N_s) was estimated on the basis of CO chemisorption values, assuming spherical metal particles. N_s for each tested catalyst was measured by CO-pulse chemisorption (BELCAT-A, BEL, Japan) at 50 °C using a He flow of 30 mL min⁻¹ and pulses of 0.09 mL (9.88% CO in He).⁷ Prior to these measurements, the catalyst after the reaction was heated with flowing He (50 mL min⁻¹) at 300 °C for 1 h. The stoichiometry of the transition metal/CO was assumed to be 1. N_s for BaH₂-BaO/Fe/CaH₂ was estimated to be 7.2×10^{16} atoms g⁻¹ from CO-pulse chemisorption experiments. The amount of saturated CO adsorption on the iron catalyst was also measured using a closed gas circulation and evacuation system. There was no difference in N_s between these two methods.

In the estimation of each reaction order in the rate equation ($r = kP\text{H}_2^\alpha PN_2^\beta P\text{NH}_3^\gamma$), the reaction order of NH₃ (γ) is estimated by measuring the NH₃ synthesis rates with varying total gas flow at constant H₂ and N₂ partial pressures.¹⁶ The reaction orders for H₂ (α) and N₂ (β) were estimated by the correlations of $\log(r) - \gamma \log(P\text{NH}_3)$ with $\log(P\text{H}_2)$ and $\log(P\text{N}_2)$,^{16,17} respectively.

2.4. ¹⁴N₂-¹⁵N₂ Isotropic Exchange Reaction. N₂ isotopic exchange was examined in a U-shaped glass reactor connected with a closed gas-circulation system. A mixture of ¹⁵N₂ and ¹⁴N₂ (total pressure: 20.0 kPa, ¹⁵N₂/¹⁴N₂ = 1:4) was adsorbed on the catalyst without circulation at the reaction temperature until adsorption/desorption was in equilibrium. The change in the composition of circulating gas was monitored by a quadrupole mass spectrometer (M-101QA-TDM, Canon Anelva Co.). The m/z = 28, 29, and 30 signals were monitored as a function of time to follow the exchange.

The formation rates for ¹⁵NH₃ and ¹⁴NH₃ over the tested catalysts were estimated under 0.1 MPa (H₂/N₂ = 3:1, WHSV: 36 000 mL g cat⁻¹ h⁻¹), although ammonia synthesis over the tested catalysts in this study was typically measured under 0.9 MPa. After ¹⁴NH₃ synthesis from ¹⁴N₂ at each reaction temperature, ¹⁴N₂ was switched to ¹⁵N₂ (98 atom% ¹⁵N, Sigma-Aldrich), and ¹⁵NH₃ was synthesized at each reaction temperature. The ¹⁴NH₃ or ¹⁵NH₃ produced were

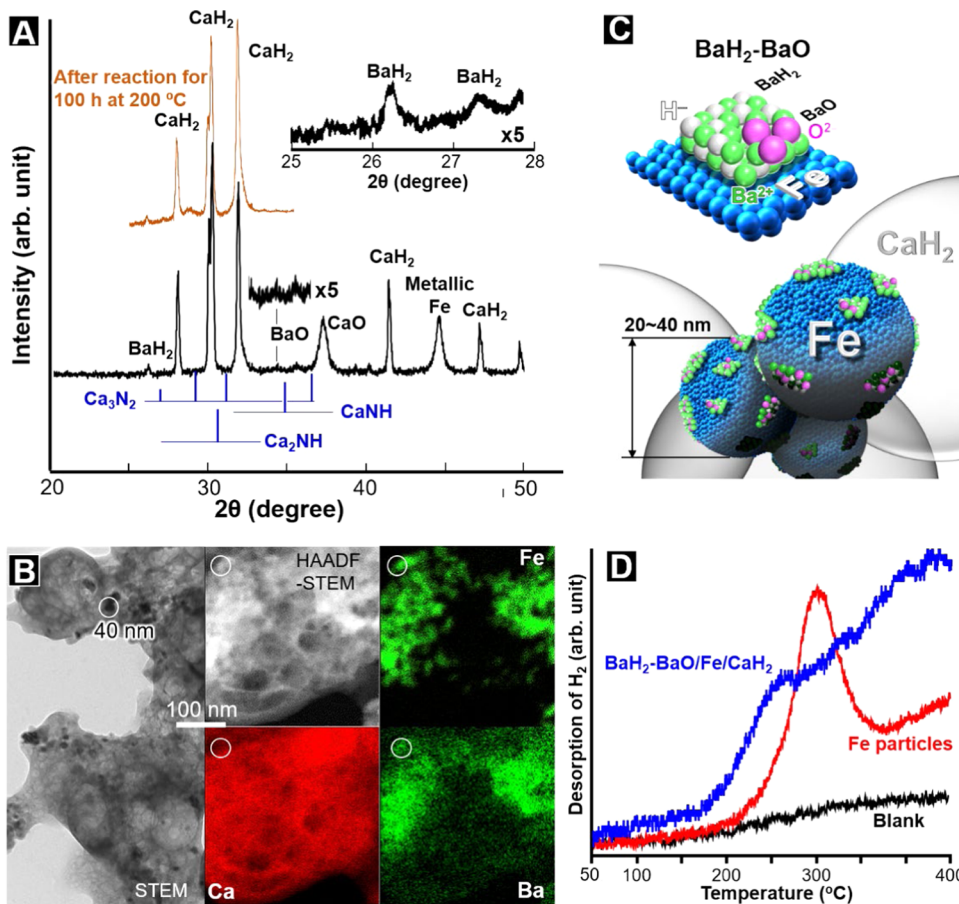


Figure 2. (A) Powder X-ray diffraction (XRD) patterns for BaH₂-BaO/Fe/CaH₂ after preparation and ammonia synthesis reaction for 100 h at 200 °C (see below). (B) High-angle annular dark-field scanning transmission electron microscopy (HAADF-STEM) and energy dispersive X-ray spectroscopy (EDX) images for BaH₂-BaO/Fe/CaH₂. (C) Schematic structure of BaH₂-BaO/Fe/CaH₂. (D) H₂ ($m/z = 2$)-TPD profiles for metallic iron particles with and without BaH₂-BaO (BaH₂-BaO/Fe/CaH₂ and Fe). Fe particles, metallic iron particles without BaO-BaH₂, were obtained by heating 0.019 g of α -Fe₂O₃, with 0.081 g of CaH₂ in a flow of H₂ (45 mL min⁻¹) at 300 °C for 2 h. After ammonia synthesis at 300 °C for over 20 h, the catalyst was cooled down to room temperature in a flow of Ar and was then heated at a rate of 1 °C min⁻¹. Desorbed H₂ was detected with a quadrupole mass spectrometer.

trapped in a 5 mM H₂SO₄ aqueous solution, and the solution was then analyzed using ion chromatography.

2.5. Characterization. Powder X-ray diffraction (XRD; Mini-flex600C, Rigaku) patterns were obtained using Cu K α radiation. Nitrogen adsorption–desorption isotherms were measured at −196 °C with a surface-area analyzer (BELSORP-mini II, MicrotracBEL) to estimate the Brunauer–Emmett–Teller (BET) surface areas. The morphologies of the samples were observed using high-angle annular dark-field scanning transmission electron microscopy (HAADF-STEM) and energy dispersive X-ray spectroscopy (EDX; JEM-ARM 200F, Jeol). H₂ and D₂-temperature-programmed desorption (TPD) profiles were measured by heating (1 °C min⁻¹) a sample (ca. 100 mg) in a flow of Ar (30 mL min⁻¹), and the concentration of H₂ and D₂ was monitored with a mass spectrometer (BELMass, MicrotracBEL, Japan). Fourier transform infrared (FT-IR) spectra were measured using a spectrometer (FT/IR-6100, Jasco) equipped with a mercury–cadmium–tellurium detector at a resolution of 4 cm⁻¹. Samples were pressed into self-supported disks. A disk was placed in a sealed and Ar-filled silica-glass cell equipped with NaCl windows to a closed gas-circulation system. The disk was heated under vacuum at 200 °C for 90 min. After the pretreatment, the disk was cooled to 25 °C under vacuum to obtain a background spectrum from the spectra of the N₂-adsorbed samples. Pure N₂ (99.99995%) was introduced into the system through a liquid nitrogen trap. X-ray photoelectron spectroscopy (XPS; ESCA-3200, Shimadzu, Mg K α , 8 kV, 30 mA) was performed in conjunction with an Ar-filled glovebox, where the samples were moved to the ultra-high vacuum XPS apparatus through

the Ar-filled glovebox without exposure to the ambient air. The binding energy was corrected with respect to the Au 4f_{7/2} peak of Au-deposited samples.

3. RESULTS AND DISCUSSION

3.1. Iron Particles Loaded with an Electron-Donating Material. In several tested catalyst designs, metallic iron particles loaded with a mixture of BaO and BaH₂ (BaH₂-BaO/Fe/CaH₂) were effective for low-temperature ammonia synthesis. Conventional supported iron catalysts, where iron nanoparticles are deposited on support particles with an electron-donating capability, cannot act as catalysts for ammonia synthesis below 200 °C. For example, an Fe nanoparticle (~4 nm)-deposited BaH₂-BaO mixture (Fe/BaH₂-BaO) did not work for ammonia synthesis, even at 300 °C, although a Ru nanoparticle-deposited BaH₂-BaO mixture (Ru/BaH₂-BaO; see Supporting Information 1.2), which is similar to Fe/BaH₂-BaO, could synthesize ammonia at low temperatures (Table S1). BaH₂-BaO/Fe/CaH₂ was readily prepared by heating Ba(NO₃)₂-impregnated Fe₂O₃ particles (20–40 nm) with CaH₂ particles at 300 °C in a flow of H₂. Figure 2A shows powder XRD profiles for BaH₂-BaO/Fe/CaH₂ immediately after preparation and after the ammonia synthesis reaction for 100 h at 200 °C (see Figure 3B). The

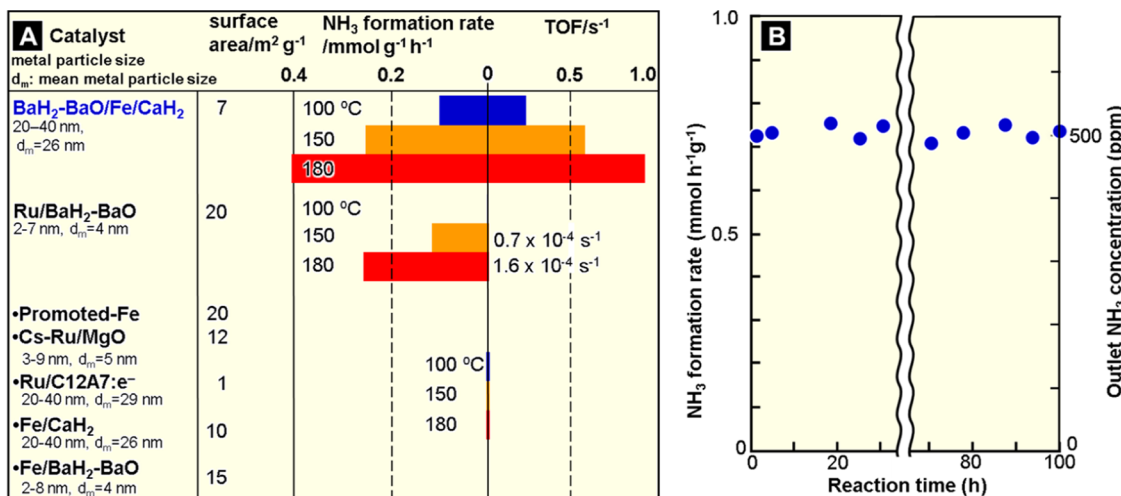


Figure 3. (A) Catalytic performance (ammonia formation rate and TOF) of the tested catalysts for ammonia synthesis at low temperatures. WHSV: 36 000 mL g⁻¹ h⁻¹, 0.9 MPa. (B) Time course of the ammonia formation rate on BaH₂-BaO/Fe/CaH₂ at 200 °C.

XRD profiles were measured in Ar without exposure of the samples to the atmosphere. Diffraction peaks due to CaCO₃ ($2\theta = 25^\circ$), calcium nitride species (Ca₃N₂, CaNH, and Ca₂NH), and barium nitride ($2\theta = 27^\circ$) did not appear in the XRD pattern for either sample. H₂O and oxygen species adsorbed on these samples, and all catalyst precursors stored in the Ar-filled glovebox were below the detection limit of mass spectrometry. Small diffraction peaks that could be assigned to BaH₂ ($2\theta = 26.3$ and 27.3° , JCPDS01-086-1744) were observed in the XRD profiles, together with those for CaH₂, CaO, and metallic iron. On the other hand, there were no clear diffraction peaks for BaO or iron oxide species such as FeO, Fe₃O₄, and Fe₂O₃.

The Ba 3d_{5/2} XPS spectrum for BaH₂-BaO/Fe/CaH₂ is shown in Figure S2. A Ba 3d_{5/2} peak appeared at 781 eV in the XPS spectrum. This peak is generally insensitive to the electronic states of Ba compounds, and the binding energy is below 780 eV for most Ba species, which includes metallic Ba and BaO, except for a few rare exceptions.^{18,19} One such exception is BaH₂, for which the binding energy for the Ba 3d_{5/2} peak is 782.9 eV.²⁰ The Ba 3d_{5/2} peak for BaH₂-BaO/Fe/CaH₂ is located at a larger binding energy than those for most Ba species; the binding energy is close to that (781.5 eV) for a BaH₂-BaO mixture obtained by heating a mixture of BaO and CaH₂.¹⁵ The Fe 2p XPS spectrum for BaH₂-BaO/Fe/CaH₂ (Figure S3) immediately after preparation showed that the iron particle surface consists of Fe⁰ (48%), Fe²⁺ (26%), and Fe³⁺ (26%). These XRD and XPS results indicate that BaH₂-BaO/Fe/CaH₂ is mainly composed of BaH₂, metallic iron, CaH₂, and CaO, and the surfaces of BaH₂ and metallic iron are partially oxidized. The BaH₂ content in the Ba species was estimated to be more than 90 mol% from XRD patterns for various physical mixtures of BaH₂ and BaO particles.

The bright-field STEM image (Figure 2B) reveals dark particles (>10–30 nm) due to either or both iron and Ba species on CaH₂. HAADF-STEM and EDX images indicated that Ba species are present together with iron particles on CaH₂; there are BaH₂-deposited metallic iron particles on CaH₂ particles in BaH₂-BaO/Fe/CaH₂, as shown in Figure 2C. In the XPS spectrum of BaH₂-BaO/Fe/CaH₂, a Ca 2p peak appeared at 347.0 eV in between those of CaH₂ (347.4 eV) and CaO (346.4 eV) (Figure S4). As a result, BaH₂-deposited

metallic iron particles come into contact with CaH₂ particles through a partially oxidized CaH₂ surface.

We have previously reported that Ru nanoparticles in contact with alkaline earth metal hydrides MH₂, such as CaH₂ and BaH₂, act as an effective catalyst for ammonia synthesis.^{12,15,21} Ru nanoparticles deposited on MH₂ abstract H atoms from the near-surface due to substantial interaction between the transition metals and H⁻, and the H atoms move to the metal nanoparticles and are desorbed as H₂ molecules to leave electrons in the H⁻ vacancies of MH₂ (MH₂ → M²⁺H_(2-x)⁻e_x⁻ + xH).²¹ The resultant M²⁺H_(2-x)⁻e_x⁻ behaves as a stable surface electride with a small work function comparable to those of metallic Li, Na, and K.^{12,21} The strong electron donation from M²⁺H_(2-x)⁻e_x⁻ to the transition metal nanoparticles enhances the cleavage of N₂ molecules, which leads to high catalytic performance for ammonia synthesis. For this reason, the temperature at which H₂ begins to desorb corresponds to that at which NH₃ begins to desorb from the catalyst.^{12,15} This was confirmed on Ca²⁺H₂⁻ (Ru/CaH₂), a Ba²⁺H₂⁻-BaO mixture (Ru/BaH₂-BaO), and Ca²⁺F⁻H⁻ (Ru/CaFH) loaded with Ru nanoparticles.^{12,15} A large increase in H adatoms on the metal surface results in the spillover of H adatoms to electrons in the H⁻ vacancies of MH₂, which forms H⁻ anions (M²⁺H_(2-x)⁻e_x⁻ + xH → MH₂).⁷ H₂-TPD measurements revealed that BaH₂-BaO/Fe/CaH₂ desorbs H₂ above about 100 °C (Figure 2D), which implies that BaH₂-BaO/Fe/CaH₂ has strong electron-donating power at ≥100 °C. On the other hand, H₂ was desorbed above 200 °C from Fe/CaH₂ with metallic iron particles and without BaH₂. The H₂ desorption was due to H⁻ in CaH₂ (see Supporting Information 1.3), and no ammonia formation was observed over metallic iron particle-deposited CaH₂ (Fe/CaH₂) at 200 °C (see Figure 3A). The XRD profile for Fe/CaH₂ contained peaks due to CaH₂, CaO, and metallic iron and coincided with that for BaH₂-BaO/Fe/CaH₂, except that the former lacked diffraction peaks due to BaH₂. From these results, H₂ desorption from BaH₂-BaO/Fe/CaH₂ below 200 °C can be attributed to BaH₂ or/and CaH₂ in the presence of BaH₂. The work function for the (001) surfaces of Ba hydride species with hydride defects (Ba²⁺H_(2-1/9)⁻e_{1/9}⁻) was calculated to be 2.6 eV by density functional theory (DFT) (Figure S5). This value is smaller than that ($\Phi = 3.3$ eV) for Ca hydride species with

Table 1. Outlet Ammonia Concentrations and Spacetime Yields for BaH₂-BaO/Fe/CaH₂ and Commercial Promoted-Fe (0.9 MPa, H₂/N₂ = 3:1, WHSV: 36 000 mL g cat⁻¹ h⁻¹)

catalyst	temperature/°C	outlet NH ₃ conc. (%) (STY/kgNH ₃ kg-cat ⁻¹ h ⁻¹) ^a	theoretical outlet NH ₃ conc. (%) (STY/kgNH ₃ kg-cat ⁻¹ h ⁻¹) ^a
BaFL-BaO/Fe/CaH ₂	300	0.353 (0.86)	14.5 (35.2)
	200	0.050 (0.12)	48.6 (118.0)
	100	0.007 (0.02)	93.0 (225.8)
commercial promoted-Fe ^b	300	0.383 (0.93)	14.5 (35.2)
	200	—	48.6 (118.0)
	100	—	93.0 (225.8)

^aSpacetime yield. ^bOutlet NH₃ concentration of commercial promoted-Fe catalyst reaches 28% at 450 °C under 10 MPa (STY: 755.5 kgNH₃ kg-cat⁻¹ h⁻¹). This is consistent with the theoretical NH₃ concentration.

hydride defects (Ca²⁺H_(2-1/9)⁻e_{1/9}⁻)¹⁵ comparable to those for metallic K and Na (Φ = 2.3 and 2.4 eV, respectively). Based on the work function, H₂ release from BaH₂, followed by the formation of Ba hydride species with hydride defects, is more effective for strong electron-donating power.

3.2. Catalytic Performance of BaH₂-BaO/Fe/CaH₂ for Ammonia Synthesis. Figure 3A shows the catalytic performance for ammonia synthesis (100–200 °C, 0.9 MPa) over BaH₂-BaO/Fe/CaH₂ and Ru/BaH₂-BaO. In Ru/BaH₂-BaO, Ru metal nanoparticles (2–7 nm) are deposited on BaH₂-BaO phase formed on CaH₂ large particles (several 30 μm).¹⁵ The results for a commercial promoted iron catalyst (promoted-Fe) that consists of Fe, K₂O, Al₂O₃, and CaO, MgO loaded with Ru nanoparticles and Cs oxide species (Cs-Ru/MgO), and Ru nanoparticles deposited on [Ca₂₄Al₂₈O₆₄]⁴⁺(e⁻)₄ (Ru/C₁₂A₇:e⁻) as benchmark catalysts are also shown. Table S1 summarizes the ammonia synthesis activities (300 °C, 0.9 MPa) of the tested materials and representative catalysts with physicochemical information, including metal particle sizes and surface areas. The promoted-Fe catalyst, which was first found by Haber, Bosch, and Mittasch more than 100 years ago and has been improved since then, is not inferior to most of the recently reported catalysts; only a handful of recent catalysts surpass the iron catalyst in terms of ammonia synthesis activity (Table S1).^{8,15,22,23} Nevertheless, the rate of ammonia formation for promoted-Fe below 300 °C was lower than that estimated by an Arrhenius equation, and the difference increased with decreasing temperature.¹² Finally, promoted-Fe could not form ammonia at 200 °C. Cs-Ru/MgO and Ru/C₁₂A₇:e⁻ also did not work for ammonia synthesis below 200 °C. In contrast, BaH₂-BaO/Fe/CaH₂ revealed that iron can catalyze ammonia synthesis even at 100 °C. The rate of ammonia formation increased with the reaction temperature. Ammonia formation proceeded over BaH₂-BaO/Fe/CaH₂ without a significant decrease in activity for over 100 h (Figure 3B). The XRD profile for the catalyst after the long-term reaction is also shown in Figure 2A. There was no large difference in the XRD pattern between the catalyst after preparation and that after reaction for 100 h, which means that the catalyst structure, including CaH₂ and BaH₂, is stable during the reaction. The Fe 2p XPS spectrum for BaH₂-BaO/Fe/CaH₂ after the reaction showed that the iron particle surfaces consist of Fe⁰ (53%), Fe²⁺ (30%), and Fe³⁺ (17%); the Fe⁰/Fe²⁺/Fe³⁺ atomic ratio on the iron surfaces after the reaction was similar to that (Fe⁰/Fe²⁺/Fe³⁺ = 48:26:26) for the catalyst immediately after preparation. Taking into account the number of zero-valent Fe atoms on the iron surface of the catalyst, the reaction for 100 h was estimated to give a turnover number of ca. 600 thousand (6.12 × 10⁵); BaH₂-BaO/Fe/CaH₂ with a new type of catalyst structure acts as a stable catalyst. Table 1 summarizes the outlet ammonia concentrations and ammonia spacetime yields for the BaH₂-BaO/Fe/CaH₂ and commercial promoted-Fe catalysts, in addition to the theoretical outlet ammonia concentrations at 100, 200, and 300 °C. The outlet ammonia concentrations for both iron catalysts were considerably smaller than the equilibrium ammonia concentration. While the ammonia concentration for the former catalyst increased in proportion to the catalyst weight, an increase in catalyst weight did not lead to ammonia detection over the latter commercial iron catalyst below 200 °C.

Next, CaH₂, BaH₂, Fe/CaH₂, and BaH₂-BaO/Fe/CaH₂ were examined under ammonia synthesis conditions (0.9 MPa, 200 °C). CaH₂ and BaH₂ did not synthesize ammonia at 200 °C, as shown in Table 2. XRD analysis indicated that nitrogen-

Table 2. Ammonia Formation Rates for the Tested Samples (0.9 MPa, 200 °C, WHSV: 36 000 mL g⁻¹ h⁻¹, N₂/H₂ = 1:3)

sample	CaH ₂	BaH ₂	Fe/CaH ₂	BaH ₂ -BaO/Fe/CaH ₂
ammonia formation rate/μmol g ⁻¹ h ⁻¹	—	—	—	720

containing species such as metal nitrides, imides, and amides were not formed on any of the samples after the experiment. Therefore, these alkaline earth metal hydrides themselves cannot react with N₂ and are not effective for ammonia synthesis from H₂ and N₂ under the present reaction conditions. In ammonia synthesis catalytic systems where alkali metal and alkaline earth metal hydrides directly form ammonia, XRD diffraction peaks due to these metal nitride species are observed on the catalysts after reaction because ammonia has a high reactivity with alkali metal and alkaline earth metal hydrides, and ammonia formation on the metal hydride surfaces readily forms metal nitrides or imides.^{9,10} On the other hand, nitrogen-containing alkaline earth metal species were not detected on BaH₂-BaO/Fe/CaH₂, even after an ammonia synthesis reaction for 100 h, as described in Section 3.1. No formation of nitrogen-containing alkaline earth metal species on BaH₂-BaO/Fe/CaH₂, CaH₂, and BaH₂ under ammonia synthesis conditions and the lack of reactivity of alkaline earth metal hydrides with N₂ imply that ammonia formation, i.e., N₂ cleavage and the formation of NH_n species do not proceed on alkaline earth metal hydrides in BaH₂-BaO/Fe/CaH₂; metallic iron on the catalyst directly synthesizes ammonia, as in the case of conventional transition metal catalysts. H₂ desorption from low temperature on BaH₂-BaO/Fe/CaH₂ (Figure 2D) indicates the formation of hydride defect-containing alkaline earth metal hydride species with

strong electron-donating capability that can facilitate N₂ dissociative adsorption on transition metal surfaces. The strong electron donation by such electron-donating species due to BaH₂ or/and CaH₂ can enhance the catalytic activity of metallic iron.

Although transition metal particles on alkali metal and alkaline earth metal hydrides such as Co/LiH and Ru/CaH₂ have been reported to exhibit higher catalytic performance for ammonia synthesis than transition metal particles on metal oxides,^{9,21} Fe/CaH₂ did not form ammonia at the reaction temperature (Table 2). There is no substantial difference in the structures of BaH₂-BaO/Fe/CaH₂ and Fe/CaH₂, except that BaH₂ is not deposited on the metallic iron particles in the latter. From these results, the catalytic activity of metallic iron on BaH₂-BaO/Fe/CaH₂ is expected to be enhanced by BaH₂ or/and CaH₂ in the presence of BaH₂. In the latter case, CaH₂ acts as not only a support for metallic iron particles but also an electron-donating material and is correlated with metallic iron through BaH₂. We cannot distinguish between the two possible mechanisms because we are not able to prepare only BaH₂-deposited metallic iron particles without using CaH₂ at present.

A notable feature in Figure 3A is the catalytic activity and efficiency for ammonia formation of Ru/BaH₂-BaO. Ru/BaH₂-BaO above 300 °C is of the highest standard, as shown in Table S1.¹⁵ However, Ru/BaH₂-BaO could not synthesize ammonia at 100 °C, and the ammonia formation rate was inferior to BaH₂-BaO/Fe/CaH₂ below 200 °C, although both catalysts use the same electron-donating material. The difference is further emphasized with respect to the ammonia formation turnover for the surface zero-valent Fe and Ru atoms (turnover frequency; TOF). In Figure 3A, BaH₂-BaO/Fe/CaH₂ exhibits TOFs that are several thousand times higher than Ru/BaH₂-BaO. In heterogeneous catalysts that adopt Ru, Co, and Ni as the active sites for ammonia synthesis, the maximum TOF is at most less than 0.17 s⁻¹, even at 400 °C (Table S2).¹¹ However, the TOF of the iron catalyst was 0.23 s⁻¹ at 100 °C and reached 12.3 s⁻¹ at 300 °C. To understand the difference in catalysis between Fe and Ru promoted by the same electron-donating material, the correlation of ammonia formation rate with total pressure and the reaction orders in the rate equation on BaH₂-BaO/Fe/CaH₂ and Ru/BaH₂-BaO were measured at 200 °C and are summarized in Figure 4. The ammonia formation rate for Ru/BaH₂-BaO did not increase with increasing pressure, and the reaction order for H₂ showed a negative value of -1.6; an increase in reactant concentration cannot lead to an increase in product formation. These results are inconsistent with kinetics theory and are clearly due to hydrogen-poisoning,^{13,14} where the Ru surface on Ru/BaH₂-BaO is severely poisoned by H adatoms and cannot exhibit satisfactory catalytic performance for ammonia formation. Such a hydrogen-poisoned Ru surface would not show a high TOF. On the other hand, the rate of ammonia formation increased in proportion to the pressure over BaH₂-BaO/Fe/CaH₂ to show a positive value of +1.5 as the reaction order for H₂. As a result, the iron catalyst is not strongly affected by hydrogen-poisoning, even at 200 °C, which results in a much higher TOF than those of Ru-based catalysts. One possible explanation for hydrogen-poisoning due to the H₂ adsorption/desorption equilibrium on transition metals is the density and strength of the bonds between H adatoms and surface transition metal atoms. A larger amount of H atoms is adsorbed on transition metal surfaces with decreasing temper-

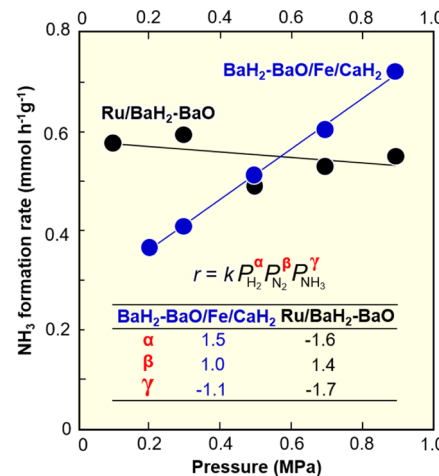


Figure 4. Correlation of the ammonia formation rate with pressure and the reaction orders for H₂, N₂, and NH₃ over BaH₂-BaO/Fe/CaH₂ and Ru/BaH₂-BaO at 200 °C.

ature; therefore, we may clarify the effect of hydrogen-poisoning by observing H₂ desorption from BaH₂-BaO/Fe/CaH₂ and Ru/BaH₂-BaO at low temperatures. Figure 5 shows

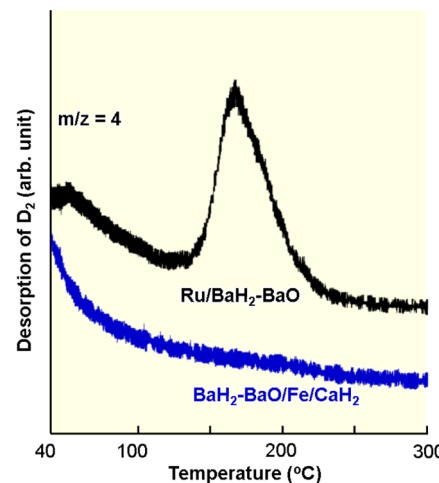


Figure 5. D₂-TPD (1 °C min⁻¹) for BaH₂-BaO/Fe/CaH₂ and Ru/BaH₂-BaO. The catalysts were heated at 300 °C in a flow of Ar to remove H adatoms from the Fe and Ru surfaces. After they were cooled down to 25 °C, D adatoms were adsorbed onto the Fe and Ru surfaces in a flow of D₂ (15 mL min⁻¹, 30 min) at 25 °C.

molecular deuterium (D₂)-TPD measurements for both the catalysts. The desorption of D adatoms due to gas-phase D₂ can be distinguished from the desorption of H adatoms originated from H⁻ anions in BaH₂ through transition metals by the use of D₂-TPD. Most D adatoms are desorbed as D₂ from the iron catalyst at 40–100 °C (see Supporting Information 1.4). It was confirmed that D₂ desorption from the iron catalyst is consistent with H₂ desorption from a single-crystal iron surface.²⁴ This suggests that the iron surface provides sufficient adsorption sites for N₂ and N adatoms without a strong influence of hydrogen-poisoning under ammonia synthesis conditions above 100 °C. In the case of Ru/BaH₂-BaO, a large D₂ desorption peak was observed at 125–225 °C; Ru binds to H adatoms more tightly than iron, and these H adatoms can cause hydrogen-poisoning on Ru over a broad temperature range. Co and Ni surfaces have also

been found to strongly adsorb H adatoms that are desorbed as H₂ at >150–200 °C as with Ru.^{25–27} These results imply that many transition metals used to synthesize ammonia can be significantly affected by hydrogen-poisoning at low temperatures, and iron is an exceptional transition metal that prevents hydrogen-poisoning. The difference in hydrogen-poisoning may be expressed as the difference in TOF among BaH₂-BaO/Fe/CaH₂ and the other transition metal-based catalysts.

3.3. Reaction Mechanism of Ammonia Formation over BaH₂-BaO/Fe/CaH₂. Ammonia synthesis over the iron catalyst was further studied to understand the reaction mechanism. Figure 6 is an energy diagram estimated from

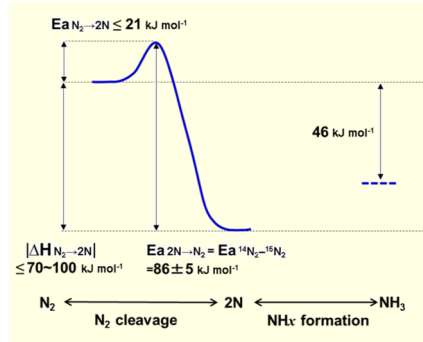


Figure 6. Potential energy diagram for dissociative N₂ adsorption on BaH₂-BaO/Fe/CaH₂.

the heat of dissociative adsorption of N₂ ($\Delta H N_2 \rightarrow 2N$) and the activation energy for N₂ desorption from N adatoms (Ea $2N \rightarrow N_2$) on BaH₂-BaO/Fe/CaH₂. Figures S6 and S7 are Arrhenius plots for ammonia synthesis and the ¹⁴N₂-¹⁵N₂ isotopic exchange reaction (¹⁴N₂ + ¹⁵N₂ ↔ 2¹⁴N¹⁵N) over BaH₂-BaO/Fe/CaH₂, respectively. From Figure S7, the ¹⁴N₂-¹⁵N₂ isotopic exchange reaction (Ea ¹⁴N₂-¹⁵N₂) was estimated to be 86 ± 5 kJ mol⁻¹. It has been confirmed that the apparent activation energy for the N₂ isotopic exchange reaction is equal to the activation energy for N₂ desorption (Ea $2N \rightarrow N_2$) by the recombination of N adatoms on ammonia synthesis heterogeneous catalysts.^{28–30} Therefore, the rate-determining step for the N₂ isotopic exchange reaction is the same as the activation energy for the recombination of N adatoms (Ea ¹⁴N₂-¹⁵N₂ = Ea $2N \rightarrow N_2$ = 86 ± 5 (81–91) kJ mol⁻¹). The dissociative adsorption heat for N₂ into N adatoms ($\Delta H N_2 \rightarrow 2N$) on a pure iron surface has been estimated to be -70 to -100 kJ mol⁻¹.³¹ Electron donation from BaH₂ to N adatoms stabilizes these atoms, which results in larger dissociative adsorption heat on BaH₂-BaO/Fe/CaH₂ than that on pure Fe.^{28,32} The dissociative adsorption heat of N₂ on the iron surface of BaH₂-BaO/Fe/CaH₂ ($\Delta H N_2 \rightarrow 2N$) would therefore be less than -70 to -100 kJ mol⁻¹ ($|\Delta H N_2 \rightarrow 2N| \geq 70$ – 100 kJ mol⁻¹). From these results, the activation energy for N₂ cleavage (Ea $N_2 \rightarrow 2N$) on BaH₂-BaO/Fe/CaH₂ is estimated to be below 21 kJ mol⁻¹ from Ea $2N \rightarrow N_2$ and $\Delta H N_2 \rightarrow 2N$ (Ea $N_2 \rightarrow 2N$ = Ea $2N \rightarrow N_2$ – $|\Delta H N_2 \rightarrow 2N|$). The apparent activation energy (Ea NH₃) for ammonia synthesis over BaH₂-BaO/Fe/CaH₂ was estimated to be 40 ± 5 kJ mol⁻¹ from Figure S6. Although BaH₂-BaO/Fe/CaH₂ can therefore be categorized as an ammonia synthesis catalyst with a small apparent activation energy, as shown in Table S2, the apparent activation energy does not directly reflect the activation energy for N₂ cleavage (Ea $N_2 \rightarrow 2N$).

Next, we examined the isotope effect over the iron catalyst through ¹⁵NH₃ and ¹⁴NH₃ formation from ¹⁵N₂-H₂ and ¹⁴N₂-H₂, respectively. The ratio of the dissociation probability for ¹⁵N₂ to that for ¹⁴N₂ on transition metal surfaces has been reported to be 0.72–0.79.³³ The results for ¹⁵NH₃ and ¹⁴NH₃ formation over BaH₂-BaO/Fe/CaH₂ in respective flows of ¹⁵N₂-H₂ and ¹⁴N₂-H₂ are summarized in Table 3. There was no

Table 3. Formation Rates of ¹⁵NH₃ and ¹⁴NH₃ over BaH₂-BaO/Fe/CaH₂ in a Flow of ¹⁵N₂-H₂ and ¹⁴N₂-H₂, Respectively (0.1 MPa, WHSV: 36 000 mL g⁻¹ h⁻¹, N₂/H₂ = 1:3)

temperature/°C	NH ₃ formation rate/mmol g ⁻¹ h ⁻¹		$r^{15}\text{NH}_3$	$r^{14}\text{NH}_3$
	r ¹⁵ NH ₃	r ¹⁴ NH ₃		
200	0.35	0.38	0.92	
250	0.59	0.58	1.02	
300	1.25	1.28	0.98	

significant difference in the ammonia formation rates between ¹⁵N₂-H₂ and ¹⁴N₂-H₂ over the iron catalyst at 200–300 °C. Many years of research, including microkinetics, iron single-crystal surfaces, and isotope experiments, indicate that N₂ dissociation is the dominant process for ammonia synthesis over iron catalysts.^{34,35} On the other hand, the results in Table 3 suggest that ammonia synthesis over BaH₂-BaO/Fe/CaH₂ cannot be simply explained only by the reaction mechanism for conventional iron catalysts.

These results may indicate facile N₂ cleavage on BaH₂-BaO/Fe/CaH₂ by weakening of the strong N≡N triple bonds. This requires electron donation from electron-donating materials to the antibonding π^* orbitals of the adsorbed N₂ via transition metal d-orbitals (*i.e.*, back-donation) to be boosted. The strong back-donation would weaken the N≡N stretching vibration by elongation of the N≡N bond. In this study, Fourier transform infrared (FT-IR) spectroscopy measurements using ¹⁴N₂ and ¹⁵N₂ as probe molecules were used to observe the N≡N stretching of N₂ adsorbed on transition metal surfaces. In the FT-IR spectrum for ¹⁴N₂ adsorbed on Ru nanoparticles deposited on Al₂O₃ (Ru/Al₂O₃) (Figure 7), the N≡N stretching band (ν N₂) appeared at 2150–2250 cm⁻¹ (peak

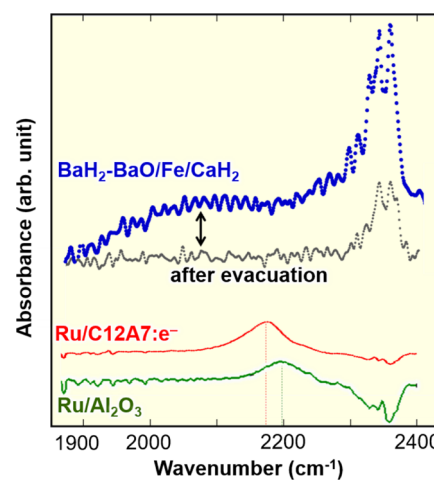


Figure 7. FT-IR spectra for N₂-adsorbed BaH₂-BaO/Fe/CaH₂, Ru/C12A7: e^- , and Ru/Al₂O₃. 10 kPa of N₂ at 25 °C.

top: 2200 cm^{-1}), which is much lower than that of gaseous N_2 (2744 cm^{-1}). The large red shift indicates that the electron donation from Ru to the antibonding π^* orbitals of adsorbed N_2 elongates the $\text{N}\equiv\text{N}$ bond. The νN_2 band was further red-shifted to 2100–2200 cm^{-1} (peak top: 2175 cm^{-1}) in the spectrum for N_2 adsorbed on Ru/C12A7: e^- , where the energy barriers for N–H species formation are larger than that of N_2 cleavage. The stronger electron donation from C12A7: e^- to N_2 molecules adsorbed on Ru facilitates the generation of N adatoms and reduces the activation energy for the latter below those for the former.²⁸ The FT-IR spectrum for $^{14}\text{N}_2$ -adsorbed BaH₂-BaO/Fe/CaH₂ in Figure 7 shows that a broad band is observed in the range of 2000–2175 cm^{-1} , which is lower than that of Ru/C12A7: e^- , and disappears after the removal of N adatoms by evacuation. The broad band was assigned to νN_2 by the $^{15}\text{N}_2$ adsorption experiment (Figure S8). Thus, the iron catalyst is more electron-donating than Ru/C12A7: e^- and can split adsorbed N_2 molecules more easily than the latter. H₂ desorption from low temperatures on BaH₂-BaO/Fe/CaH₂ (Figure 2D) indicates the formation of hydride defect-containing alkaline earth metal hydride species with strong electron-donating capability; the strong electron-donating power of the iron catalyst can be attributed to the formation of such hydride species.

As a summary of these results, the mechanism postulated for ammonia synthesis over BaH₂-BaO/Fe/CaH₂ is shown schematically in Figure 8. Only BaH₂-BaO/Fe/CaH₂, BaH₂

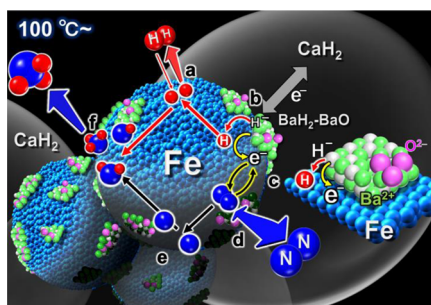


Figure 8. Schematic of the reaction mechanism for ammonia synthesis over BaH₂-BaO/Fe/CaH₂.

deposited metallic iron particles on CaH₂ particles, catalyzed ammonia synthesis at low temperatures in the tested catalyst designs that adopted iron as the active sites. The catalyst designs based on conventional supported metal catalysts, including the iron nanoparticles-deposited BaH₂-BaO mixture (Fe/BaH₂-BaO), were not effective for low-temperature ammonia synthesis. The experimental results imply that ammonia formation, including N_2 cleavage and the formation of NH_n species, proceeds on the metallic iron surface of BaH₂-BaO/Fe/CaH₂ as with ammonia synthesis over conventional transition metal catalysts. Most H adatoms on the iron surfaces desorb as H₂ below 100–150 °C (Figure 5) so that H₂ adsorption/desorption equilibrium is shifted toward H₂ desorption at low temperatures (Figure 8a). For this reason, the H adatom concentration is not so high over the entire reaction temperature range above 100–150 °C. The low H adatom concentration induces the alkaline earth metal hydride MH₂ to exhibit strong electron-donating capability. The iron surface in contact with MH₂ can abstract H atoms from MH₂ and release them as H₂ molecules ($\text{MH}_2 \leftrightarrow \text{M}^{2+}\text{H}_{(2-x)}^-\text{e}_x^- + x/2\text{H}_2$). This forms alkaline earth metal hydride species with

electrons and hydride defects ($\text{M}^{2+}\text{H}_{(2-x)}^-\text{e}_x^-$) that exhibit strong electron-donating capability. The strong electron donation to metallic iron is considered to be due to BaH₂ or/and a combination of BaH₂ and CaH₂. In the latter case, electrons derived from CaH₂ would be correlated with the metallic iron surface through BaH₂ (Figure 8). In either case, electron donation from BaH₂, as shown in Figure 8b,c, may play an important role in enhancing the catalytic activity of metallic iron. The shift of the H₂ adsorption/desorption equilibrium toward H₂ desorption on the iron surfaces would not only give the strong electron-donating capability to BaH₂ but also provide sufficient adsorption sites for N_2 molecules on the iron surface (Figure 8d). Electrons are transferred from the resulting alkaline earth metal hydride species with hydride defects to N_2 molecules adsorbed on iron surfaces. FT-IR measurements (Figure 7) revealed that the antibonding π^* orbitals of adsorbed N_2 are significantly stimulated by the strong electron donation. The strong electron donation can facilitate the cleavage of adsorbed N_2 to N adatoms (Figure 8d,e). The generated N adatoms react with H adatoms to form ammonia through the formation of N–H_n species (Figure 8f). These reactions on BaH₂-BaO/Fe/CaH₂ proceed at more than ca. 100 °C (Figure 3A) while hydrogen-poisoning is prevented. On the other hand, other transition metals such as Ru have tightly adsorbed H adatoms on their surfaces that cannot be easily removed as H₂ below 150–200 °C. The H adatoms would reduce the number of the adsorption sites for N_2 molecules and N adatoms and affect the reaction over the entire temperature range.

4. CONCLUSIONS

The present study demonstrates that metallic iron particles can catalyze ammonia synthesis from H₂ and N₂ at 100 °C in combination with BaH₂. The iron catalyst exhibits a much higher TOF than heterogeneous catalysts with other transition metals as the reaction sites. This can be attributed to the intrinsic nature of the metallic iron surface to desorb H adatoms as H₂ molecules at low temperatures of <100 °C. Many transition metals used to synthesize ammonia, such as Ru, Co, and Ni, bind to H adatoms more tightly than iron, and these H adatoms can cause hydrogen-poisoning on these transition metals over a broad temperature range >150–200 °C. As a result, iron is considered to be an exceptional transition metal that prevents hydrogen-poisoning. Strong electron donation to metallic iron particles in the presence of BaH₂ also makes a significant contribution to low-temperature ammonia formation over the iron catalyst, which indicates that alkaline metal hydride can enhance the catalytic performance of iron. Therefore, iron, which was first found to catalyze ammonia formation at high temperatures by Mittasch over 100 years ago, may also be effective for low-temperature ammonia synthesis.

■ ASSOCIATED CONTENT

SI Supporting Information

The Supporting Information is available free of charge at <https://pubs.acs.org/doi/10.1021/jacs.2c13015>.

Additional discussion, XPS spectra, DFT calculation, and FT-IR spectra (PDF)

AUTHOR INFORMATION

Corresponding Author

Michikazu Hara – Laboratory for Materials and Structures, Tokyo Institute of Technology, Yokohama 226–8503, Japan; orcid.org/0000-0003-3450-5704; Email: mhara@msl.titech.ac.jp

Authors

Masashi Hattori – Laboratory for Materials and Structures, Tokyo Institute of Technology, Yokohama 226–8503, Japan; orcid.org/0000-0002-0644-5137

Natsuo Okuyama – Laboratory for Materials and Structures, Tokyo Institute of Technology, Yokohama 226–8503, Japan

Hiyori Kurosawa – Laboratory for Materials and Structures, Tokyo Institute of Technology, Yokohama 226–8503, Japan

Complete contact information is available at:

<https://pubs.acs.org/10.1021/jacs.2c13015>

Notes

The authors declare no competing financial interest.

ACKNOWLEDGMENTS

This work was supported by a fund from the Grants-in-Aid for Japan Society for the Promotion of Science (JSPS) Fellows and for Scientific Research from the Ministry of Education, Culture, Science, Sports, and Technology (MEXT) of Japan (18H05251, 21H04630).

REFERENCES

- (1) Song, P.; Kang, L.; Wang, H.; Guo, R.; Wang, R. Nitrogen (N), phosphorus (P)-codoped porous carbon as a metal-free electrocatalyst for N₂ reduction under ambient conditions. *ACS Appl. Mater. Interfaces* **2019**, *11*, 12408–12414.
- (2) Hara, M.; Kitano, M.; Hosono, H. Ru-loaded C12A7:e⁻ electride as a catalyst for ammonia synthesis. *ACS Catal.* **2017**, *7*, 2312–2324.
- (3) Smith, C.; Hill, A. K.; Torrente-Murciano, L. Current and future role of Haber-Bosch ammonia in a carbon-free energy landscape. *Energy Environ. Sci.* **2020**, *13*, 331–344.
- (4) Rouwenhorst, K. H. R.; Van der Ham, A. G. J.; Mul, G.; Kersten, S. R. A. Islanded ammonia power systems: Technology review & conceptual process design. *Renewable Sustainable Energy Rev.* **2019**, *114*, No. 109339.
- (5) Ghavam, S.; Vahdati, M.; Wilson, I. A. G.; Styring, P. Sustainable ammonia production processes. *Front. Energy Res.* **2021**, *9*, No. 580808.
- (6) NH3 Fuel Association. <http://nh3fuelassociation.org/2013/08/28/ammonia-production-using-wind-energy/> (accessed December 1, 2022).
- (7) Kitano, M.; Inoue, Y.; Yamazaki, Y.; Hayashi, F.; Kanbara, S.; Matsuishi, S.; Yokoyama, T.; Kim, S. W.; Hara, M.; Hosono, H. Ammonia synthesis using a stable electride as an electron donor and reversible hydrogen store. *Nat. Chem.* **2012**, *4*, 934–940.
- (8) Kitano, M.; Inoue, Y.; Sasase, M.; Kishida, K.; Kobayashi, Y.; Nishiyama, K.; Tada, T.; Kawamura, S.; Yokoyama, T.; Hara, M.; Hosono, H. Self-organized ruthenium-barium core-shell nanoparticles on a mesoporous calcium amide matrix for efficient low-temperature ammonia synthesis. *Angew. Chem.* **2018**, *130*, 2678–2682.
- (9) Wang, P. K.; Chang, F.; Gao, W. B.; Guo, J. P.; Wu, G. T.; He, T.; Chen, P. Breaking scaling relations to achieve low-temperature ammonia synthesis through LiH-mediated nitrogen transfer and hydrogenation. *Nat. Chem.* **2017**, *9*, 64–70.
- (10) Gao, W. B.; Wang, P. K.; Guo, J. P.; Chang, F.; He, T.; Wang, Q.; Wu, G. T.; Chen, P. Barium hydride-mediated nitrogen transfer and hydrogenation for ammonia synthesis: a case study of cobalt. *ACS Catal.* **2017**, *7*, 3654–3661.
- (11) Ye, T.-N.; Park, S.-W.; Lu, Y.; Li, J.; Sasase, M.; Kitano, M.; Tada, T.; Hosono, H. Vacancy-enabled N₂ activation for ammonia synthesis on an Ni-loaded catalyst. *Nature* **2020**, *583*, 391–407.
- (12) Hattori, M.; Iijima, S.; Nakao, T.; Hosono, H.; Hara, M. Solid solution for catalytic ammonia synthesis from nitrogen and hydrogen gases at 50°C. *Nat. Commun.* **2020**, *11*, No. 2001.
- (13) Rosowski, F.; Hornung, A.; Hinrichsen, O.; Herein, D.; Muhler, M.; Ertl, G. Ruthenium catalysts for ammonia synthesis at high pressures: Preparation, characterization, and power-law kinetics. *Appl. Catal. A* **1997**, *151*, 443–460.
- (14) Siporin, S. E.; Davis, R. J. Use of kinetic models to explore the role of base promoters on Ru/MgO ammonia synthesis catalysts. *J. Catal.* **2004**, *225*, 359–368.
- (15) Hattori, M.; Mori, T.; Arai, T.; Inoue, Y.; Sasase, M.; Tada, T.; Kitano, M.; Yokoyama, T.; Hara, M.; Hosono, H. Enhanced catalytic ammonia synthesis with transformed BaO. *ACS Catal.* **2018**, *8*, 10977–10984.
- (16) Iriawan, H.; Andersen, S. Z.; Zhang, X.; Comer, B. M.; Barrio, J.; Chen, P.; Medford, A. J.; Stephens, I. E. L.; Chorkendorff, I.; Shao-Horn, Y. Methods for nitrogen activation by reduction and oxidation. *Nat. Rev. Methods Primers* **2021**, *1*, No. 56.
- (17) Cao, A.; Bukas, V. J.; Shadravan, V.; Wang, Z.; Li, H.; Kibsgaard, J.; Chorkendorff, I.; Norskov, J. K. A spin promotion effect in catalytic ammonia synthesis. *Nat. Commun.* **2022**, *13*, No. 2382.
- (18) Lampert, W. V.; Rachocki, K. D.; Lamartine, B. C.; Haas, T. W. Electron-spectroscopic investigations of Ba and Ba compounds. *J. Electron Spectrosc. Relat. Phenom.* **1982**, *26*, 133–145.
- (19) Koenig, M. F.; Grant, J. T. XPS studies of the chemical state of Ba on the surface of impregnated tungsten dispenser cathodes. *Appl. Surf. Sci.* **1985**, *20*, 481–496.
- (20) Franzen, H. F.; Merrick, J.; Umana, M.; Khan, A. S.; Peterson, D. T.; et al. XPS spectra and crystalline potentials in alkaline-earth chalcogenides and hydrides. *J. Electron Spectrosc. Relat. Phenom.* **1977**, *11*, 439–443.
- (21) Kitano, M.; Inoue, Y.; Ishikawa, H.; Yamagata, K.; Nakao, T.; Tada, T.; Matsuishi, S.; Yokoyama, T.; Hara, M.; Hosono, H. Essential role of hydride ion in ruthenium-based ammonia synthesis catalysts. *Chem. Sci.* **2016**, *7*, 4036–4043.
- (22) Ogura, Y.; Sato, K.; Miyahara, S.; Kawano, Y.; Toriyama, T.; Yamamoto, T.; Matsumura, S.; Hosokawa, S.; Nagaoaka, K. Efficient ammonia synthesis over a Ru/La_{0.5}Ce_{0.5}O_{1.75} catalyst pre-reduced at high temperature. *Chem. Sci.* **2018**, *9*, 2230–2237.
- (23) Ogura, Y.; Tsujimura, K.; Sato, K.; Miyahara, S.; Toriyama, T.; Yamamoto, T.; Matsumura, S.; Nagaoaka, K. Ru/La_{0.5}Pt_{0.5}O_{1.75} catalyst for low-temperature ammonia synthesis. *ACS Sustainable Chem. Eng.* **2018**, *6*, 17258–17266.
- (24) Bozso, F.; Ertl, G.; Grunze, M.; Weiss, M. Chemisorption of hydrogen on iron surfaces. *Appl. Surf. Sci.* **1977**, *1*, 103–119.
- (25) Xue, X.; Liu, J.; Rao, D.; Xu, S.; Bing, W.; Wang, B.; He, S.; Wei, M. Double-active site synergistic catalysis in Ru-TiO₂ toward benzene hydrogenation to cyclohexene with largely enhanced selectivity. *Catal. Sci. Technol.* **2017**, *7*, 650–657.
- (26) Huesges, Z.; Christmann, K. Interaction of hydrogen with a cobalt(0001) surface. *Z. Phys. Chem.* **2013**, *227*, 881–889.
- (27) Znak, L.; Zielinski, J. Effects of support on hydrogen adsorption/desorption on nickel. *Appl. Catal. A* **2008**, *334*, 268–276.
- (28) Kitano, M.; Kanbara, S.; Inoue, Y.; Kuganathan, N.; Sushko, P. V.; Yokoyama, Y.; Hara, M.; Hosono, H. Electride support boosts nitrogen dissociation over ruthenium catalyst and shifts the bottleneck in ammonia synthesis. *Nat. Commun.* **2015**, *6*, No. 6731.
- (29) Hinrichsen, O.; Rosowski, F.; Hornung, A.; Muhler, M.; Ertl, G. The kinetics of ammonia synthesis over Ru-based catalysts: 1. The dissociative chemisorption and associative desorption of N₂. *J. Catal.* **1997**, *165*, 33–44.
- (30) Hayashi, F.; Toda, Y.; Kanie, Y.; Kitano, M.; Inoue, Y.; Yokoyama, T.; Hara, M.; Hosono, H. Ammonia decomposition by ruthenium nanoparticles loaded on inorganic electride C12A7:e⁻. *Chem. Sci.* **2013**, *4*, 3124–3130.

- (31) Yeo, B. C.; Kong, J.; Kim, D.; Goddard, W. A., III; Park, H. S.; Han, S. S. Electronic structural origin of the catalytic activity trend of transition metals for electrochemical nitrogen reduction. *J. Phys. Chem. C* **2019**, *123*, 31026–31031.
- (32) Kuganathan, N.; Hosono, H.; Shluger, A. L.; Sushko, P. V. Enhanced N₂ dissociation on Ru-loaded inorganic electride. *J. Am. Chem. Soc.* **2014**, *136*, 2216–2219.
- (33) Haase, G.; Asscher, M.; Kosloff, R. The dissociative chemisorption dynamics of N₂ on catalytic metal surfaces: A quantum-mechanical tunneling mechanism. *J. Chem. Phys.* **1989**, *90*, 3346–3355.
- (34) Ertl, G. *Catalytic Ammonia Synthesis*, 1st ed.; Jennings, J. R., Ed.; Plenum Press: New York, 1991; p 109.
- (35) Aika, K.; Ozaki, A. Kinetics and isotope effect of ammonia synthesis over an unpromoted iron catalyst. *J. Catal.* **1969**, *13*, 232–237.

□ Recommended by ACS

Work Function-Tailored Nitrogenase-like Fe Double-Atom Catalysts on Transition Metal Dichalcogenides for Nitrogen Fixation

Xue Yao, Chandra Veer Singh, *et al.*

MARCH 22, 2023

ACS SUSTAINABLE CHEMISTRY & ENGINEERING

READ ↗

Stacking of a Cofacially Stacked Iron Phthalocyanine Dimer on Graphite Achieved High Catalytic CH₄ Oxidation Activity Comparable to That of pMMO

Yasuyuki Yamada, Kentaro Tanaka, *et al.*

JANUARY 10, 2023

JACS AU

READ ↗

Homogeneous Carbon Dot-Anchored Fe(III) Catalysts with Self-Regulated Proton Transfer for Recyclable Fenton Chemistry

Ting Zhang, Yixin Zhao, *et al.*

JANUARY 16, 2023

JACS AU

READ ↗

Revisiting the Electrochemical Nitrogen Reduction on Molybdenum and Iron Carbides: Promising Catalysts or False Positives?

Boaz Izelaar, Ruud Kortlever, *et al.*

JANUARY 12, 2023

ACS CATALYSIS

READ ↗